

## Far-infrared spectroscopy of $\text{TbPO}_4$

J. F. L. Lewis\* and G. A. Prinz

Naval Research Laboratory, Washington, D.C. 20375

(Received 8 July 1974)

A direct spectroscopic investigation has been carried out of the low-lying crystal-field states of the lowest  $J$  manifold of  $\text{Tb}^{3+}$ ,  ${}^7F_6$  in single crystals of  $\text{TbPO}_4$ , at 4.2°K. The energies and compositions of these states are of interest as a basis for understanding the subsequent phase transitions which occur as the temperature is lowered: a Jahn-Teller distortion at 3.5°K, and antiferromagnetic ordering at 2.2°K. Transitions between these states fall in the far infrared, and were studied by two techniques: interferometric spectroscopy over the region from 15 to 200  $\text{cm}^{-1}$  with 2- $\text{cm}^{-1}$  resolution, and far-infrared magnetic resonance employing molecular-gas lasers which provided 14 separate energies from 8.5 to 58.5  $\text{cm}^{-1}$ . Zeeman splittings were measured spectroscopically for both  $\vec{H} \parallel \vec{C}$  and  $\vec{H} \perp \vec{C}$ , while for the resonance measurements  $\vec{H} \parallel \vec{C}$  only. Applied fields up to 100 kOe and radiation polarized both  $\sigma$  ( $\vec{E} \perp \vec{C}$ ) and  $\pi$  ( $\vec{E} \parallel \vec{C}$ ) were employed. The detailed Zeeman behavior of the eight lowest states has been determined. At zero field, four lie below 10  $\text{cm}^{-1}$ , one at 20  $\text{cm}^{-1}$ , and three at  $\approx 80 \text{ cm}^{-1}$ . A crystal-field calculation was done to fit the Zeeman spectra, yielding crystal-field parameters, energies, and wave functions.

### I. INTRODUCTION

Rare-earth arsenates, phosphates, and vanadates of the zircon structure have recently received considerable attention because of their interesting structural behavior at low temperatures. The compounds  $R(\text{XO}_4)_3$ , where  $R = \text{Tb}^{3+}$ ,  $\text{Dy}^{3+}$ ,  $\text{Tm}^{3+}$  and  $X = \text{As}, \text{V}$ , all exhibit a cooperative Jahn-Teller distortion below 50°K, and in  $\text{DyVO}_4$ ,  $\text{DyAsO}_4$ , and  $\text{TbAsO}_4$  the distortion is followed by magnetic ordering below 5°K. Molecular-field theory has been successful in describing the distortion and/or magnetic-ordering behavior of many of these compounds.

$\text{TbPO}_4$  is less well understood. It magnetically orders at  $T_N = 2.2$ °K and there is evidence that it undergoes a Jahn-Teller crystallographic distortion at  $T_D = 3.5$ °K. The available data, however, are somewhat confusing and in part contradictory. In order to help clarify the situation, a far-infrared spectroscopic investigation was undertaken at 4.2°K, above both  $T_D$  and  $T_N$ , and in applied magnetic fields both parallel and perpendicular to the tetragonal axis  $C$ , in an effort to obtain the high-temperature energy-level structure of the  $\text{Tb}^{3+}$  ground manifold. This information is essential for an understanding of the subsequent phase transitions, in which the levels mix and shift in energy as the temperature is lowered through the two transition temperatures. A preliminary report of the results was presented at the 19th Annual Conference on Magnetism and Magnetic Materials.<sup>1</sup> In the present paper we report the results in detail.

In Sec. II we will review previous work done on  $\text{TbPO}_4$  and point out the apparent inconsistencies. In Sec. III we discuss our experimental techniques and results, which we analyze in Sec. IV. We dis-

cuss some of the previous work in the light of our conclusions in Sec. V.

### II. PREVIOUS EXPERIMENTAL WORK

$\text{TbPO}_4$  reportedly crystallizes in one of two different structures, a tetragonal phase with space group  $D_{4h}^{19}$  and a monoclinic phase.<sup>2</sup> The flux-growth technique used to produce single crystals ordinarily yields the former, and all of the recent work has been done on that phase, in which the rare-earth ions have  $D_{2d}$  site symmetry. The unit cell is shown in Fig. 1; the room-temperature lattice parameters are  $a_0 = 6.941$  Å and  $c_0 = 6.070$  Å. Each ion has four near neighbors and eight second neighbors.

Specific-heat and magnetic-susceptibility measurements<sup>3-5</sup> indicate that  $\text{TbPO}_4$  orders as an antiferromagnet at  $T_N = 2.2$ °K. Neutron scattering experiments have indicated a two-sublattice colinear structure whose antiferromagnetic axis is canted from the  $C$  axis, but two different values have been obtained for the angle,  $40^\circ \pm 1^\circ$  (Ref. 6) and  $26^\circ$ .<sup>7</sup> Early specific-heat and susceptibility measurements<sup>3,4</sup> showed no evidence of a crystallographic distortion above the magnetic-ordering temperature. Later, careful specific-heat measurements indicated a small peak above  $T_N$ , whose origin was ascribed to a distortion at  $T_D = (3.5 \pm 0.1)$ °K.<sup>5</sup> Spectroscopic investigations in the visible show that absorption lines shift to higher energy as the temperature is lowered through  $T_N$ .<sup>3,4,8,9</sup> There have been several proposals for the origin of this shift: magnetic ordering only,<sup>3,4</sup> magnetic ordering plus a possible distortion occurring at or below  $T_N$  (Ref. 8), and magnetic ordering plus a distortion occurring above  $T_N$ .<sup>9</sup>  $g$ -factor measurements at 4.2°K in applied perpendicular fields of

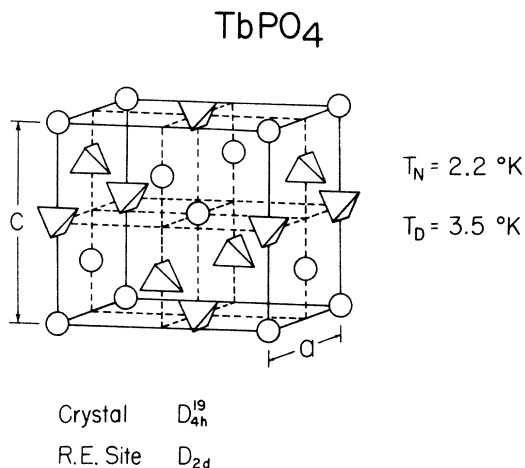


FIG. 1. High-temperature tetragonal-phase unit cell of TbPO<sub>4</sub>. The tetrahedra represent the (PO<sub>4</sub>)<sup>3-</sup> radicals; the spheres represent the Tb<sup>3+</sup> ions. The Jahn-Teller distortion temperature  $T_D$  and the Néel temperature  $T_N$  are given along with the appropriate symmetry classes.

21–35 kOe exhibit a  $\frac{1}{2}\pi$  periodicity,<sup>3,8</sup> as do perpendicular magnetization measurements at 4.2 °K for  $H > 10$  kOe.<sup>5</sup> This indicates that above  $T_D = 3.5$  °K a distortion can be induced by the application of a perpendicular magnetic field. Finally, from measurements of the magnetoelectric effect in TbPO<sub>4</sub>, it was concluded that the symmetry of TbPO<sub>4</sub> in the antiferromagnetic state is lower than tetragonal if the crystal has not been magnetoelectrically annealed.<sup>10</sup> This again indicates the presence of a distortion.

The ground manifold of the Tb<sup>3+</sup> ion is  $^7F_6$ . In TbPO<sub>4</sub> the tetragonal crystal field removes the  $J_x$  degeneracy, splitting the  $J=6$  manifold into ten levels, of which three are time-reversed doublets and seven are singlets. In this even electron system there can be no first-order parallel or perpendicular Zeeman behavior of the singlets, and no first-order perpendicular effect for the doublets.

There have been several schemes suggested for the position and character of the lowest levels of this manifold at 4.2 °K, above both the distortion and magnetic-ordering temperatures. In one optical-spectroscopy study<sup>3,8</sup> the high-field (35-kOe)  $g$ -factor for the ground state was found to be  $16 \pm 2$ , which was attributed to either a  $m_J = \pm 5$  degenerate doublet or two nearly degenerate  $m_J = 6$  singlets. A perpendicular Zeeman effect was also observed, but its origin was not discussed. A second optical study<sup>4</sup> yielded an energy scheme of a doublet and a singlet lowest, very close together, and two almost degenerate singlets at about 27 cm<sup>-1</sup>. A third optical study<sup>9</sup> was interpreted as indicating a  $m_J = \pm 5$  doublet lowest, with  $g_{\parallel} = 14 \pm 1$  ( $H = 0$ –20 kOe), a

singlet in the region 10–15 cm<sup>-1</sup>, and another singlet in the region 19–27 cm<sup>-1</sup>. The observed  $g_{\perp}$  was attributed to coupling between the doublet and the next singlet at 10–15 cm<sup>-1</sup>. Unpublished  $T = 4.2$  °K magnetization curves ( $H = 0$ –20 kOe) were fit<sup>5</sup> to a model of a doublet lowest and a singlet at 1.5 cm<sup>-1</sup>, giving  $g_{\parallel} = 12.0 \pm 0.3$  for the doublet and  $g_{\perp} = 7.1 \pm 0.2$  arising from coupling between the doublet and the singlet. Part of the discrepancies and uncertainties in the optical data result from the unusually large linewidths and line asymmetries observed.<sup>8,9</sup>

### III. EXPERIMENT

#### A. Techniques

The far-infrared studies of TbPO<sub>4</sub> were carried out on single-crystal samples grown from a PbO flux. The growth habit was rectangular prisms as illustrated in Fig. 2. For some transmission measurements several crystals were laid side by side to obtain a mosaic sample of uneven thickness on which it was nevertheless possible to obtain well-defined Zeeman and polarization measurements. The far-infrared transmission was measured by means of interferometric spectroscopy and magnetic-resonance spectroscopy. The former method employed a commercially available Michelson interferometric spectrometer<sup>11</sup> and cryogenic detectors to cover the spectral region 10 to 200 cm<sup>-1</sup>.

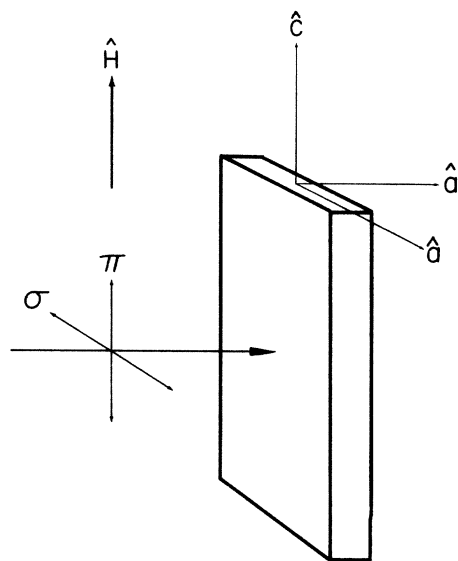


FIG. 2. Growth habit of the thin-slab samples of TbPO<sub>4</sub> with respect to the unit cell axes  $\hat{a}$ ,  $\hat{a}'$ , and  $\hat{c}$ , and the experimental orientation for transmission measurements. The magnetic field direction  $\hat{H}$  shown is for parallel Zeeman studies. Perpendicular Zeeman measurements were made with  $\hat{H} \parallel \hat{a}'$ , i. e., parallel to the optical propagation.

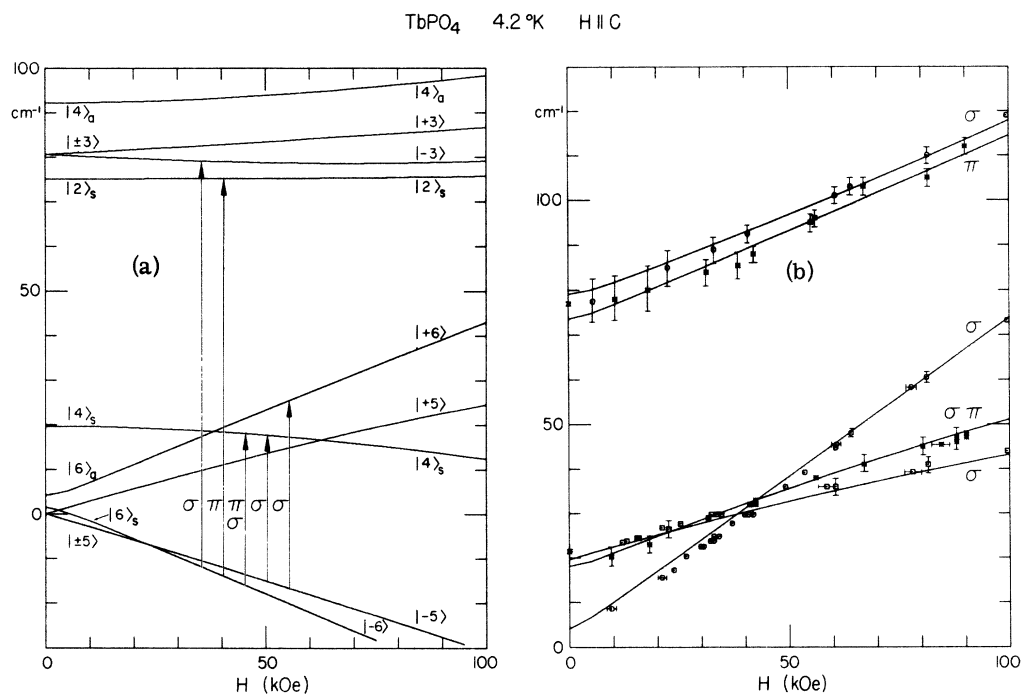


FIG. 3. (a) Calculated behavior of the crystal-field levels given by the parameters in Table II for a magnetic field applied parallel to the tetragonal axis. The arrows indicate the observed far-infrared transitions, labeled with their polarizations. The label on each state indicates its principal composition as explained in the text. (b) Calculated Zeeman behavior of the transitions as fitted to the experimentally measured spectra. The uncertainties in the resonance spectra are measured in field (i. e., horizontally) while the uncertainties in the fixed-field Zeeman spectra are measured in frequency (i. e., vertically).

The latter technique utilized far-infrared gas lasers to supply monochromatic radiation whose transmission was measured as a function of applied magnetic field. A pulsed-gas-discharge H<sub>2</sub>O/D<sub>2</sub>O laser provided 45.41 and 58.25 cm<sup>-1</sup>. An optically pumped molecular-gas laser was also used to provide 14 frequencies between 8.5 and 39.2 cm<sup>-1</sup>. This laser, of the type first reported by Chang *et al.*,<sup>12</sup> employs a carefully stabilized pulsed CO<sub>2</sub> laser to pump another laser cavity containing gaseous organic compounds. The details of this system have been described elsewhere.<sup>13</sup> The resonance data obtained at 8.5 cm<sup>-1</sup> (275 GHz) is the farthest into the infrared that has been reported using a laser source. The Zeeman studies and magnetic-resonance measurements were made in applied fields up to 105 kOe. Measurements were made for the applied field parallel as well as perpendicular to the tetragonal axis. All measurements were made at a sample temperature of 4.2°K, which is above both the Néel temperature and the reported spontaneous-distortion temperature.

#### B. Results

The results of these spectroscopic measurements are presented in Figs. 3(b) and 4(b). Five

transitions are observed in both parallel and perpendicular fields in the spectral range which we covered. In parallel fields one transition was polarized π, three were σ, and one was π plus σ. In the perpendicular Zeeman measurements no polarizers were employed. One would expect the spectra to become depolarized due to the mixing of crystal-field states. In Figs. 3(b) and 4(b), the observed spectra are represented by the data points. The error bars represent the uncertainty in locating the absorption peak. In the interferometer spectra, this uncertainty is in the energy, but in magnetic resonance the frequency is very well defined and the uncertainty is in the value of the applied field. If a particular experiment were repeated, the several values for that line are included instead of error bars. We shall first discuss the polarized data obtained for  $\vec{H} \parallel \vec{C}$  illustrated in Fig. 3(b).

In zero applied magnetic field, there is a broad absorption peak at ≈ 78 cm<sup>-1</sup>. In high applied fields the line sharpens somewhat and is seen to be two transitions, one σ, the other π, separated by ≈ 5 cm<sup>-1</sup>. Similarly, at low energies in zero applied field there is a single absorption line at ≈ 20 cm<sup>-1</sup>. This also sharpens at high fields to reveal two components, one polarized σ, the other π and σ.

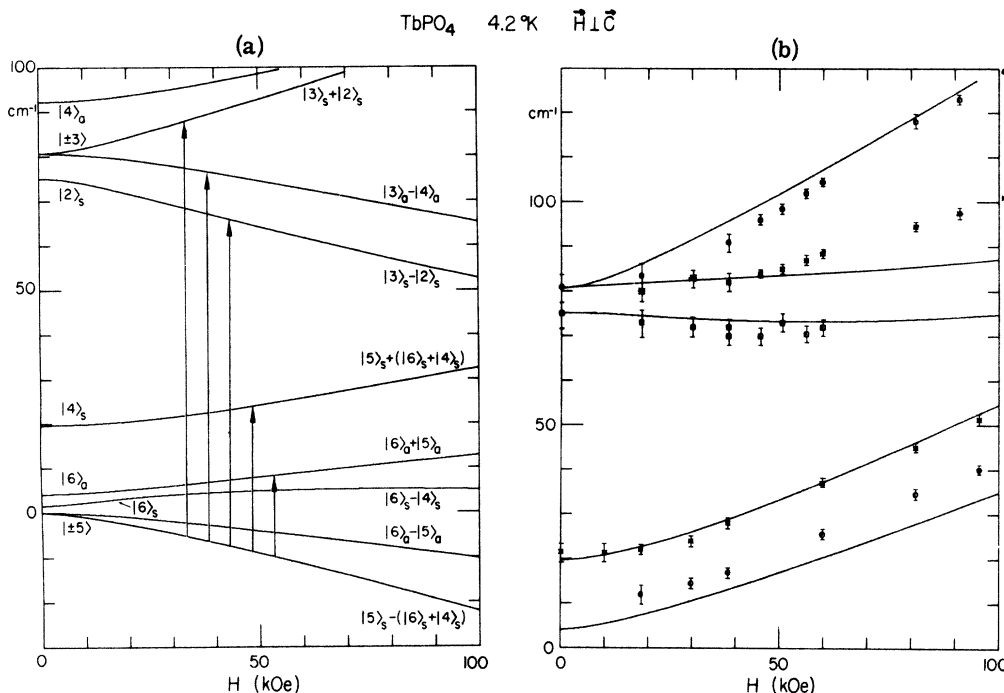


FIG. 4. (a) Calculated behavior of the crystal-field levels given by the parameters in Table II for a magnetic field applied perpendicular to the tetragonal axis. The notation is the same as used in Fig. 3(a). (b) Calculated Zeeman behavior of the transitions compared with the experimentally measured spectra. The notation is the same as used in Fig. 3(b).

The remaining transition is not seen in zero field due to the limitations of our spectral range. Its large splitting factor enables it to be moved readily, and it is seen by magnetic resonance at  $8.5 \text{ cm}^{-1}$  in an applied field of 9 kOe. This transition is the sharpest ( $\Delta H = 8 \text{ kOe}$ ) throughout the region studied and is  $\sigma$  polarized.

The unpolarized data obtained for  $\vec{H} \perp \vec{C}$  are shown in Fig. 4(b). The applied magnetic field was perpendicular to the large face of the crystal platelets. X-ray orientation has shown this to be along an  $a$  axis of the unit cell, as shown in Fig. 2. Again we have five transitions, but now there are three at higher energies and two at low energies. The three higher-energy transitions only become resolved as they spread apart and sharpen in sufficiently high fields. The upper two lines strengthen with increasing field, but the third moves very little with field, weakens and finally disappears at  $H > 60 \text{ kOe}$ . The line at  $\approx 20 \text{ cm}^{-1}$  moves slowly with field and a line originating below  $10 \text{ cm}^{-1}$  again moves upward and into our experimental spectral region, moving roughly parallel to the one above it. The 75- and 81- $\text{cm}^{-1}$  transitions at  $H_1 = 0$  were resolved in the thinner samples used for the perpendicular Zeeman studies, but not in the thicker samples used for the parallel ones.

#### IV. ANALYSIS

The task is to understand this observed Zeeman behavior of the far-infrared spectra in a scheme which is compatible with the optical spectra reported by others. Since the evidence indicates that the crystal may be distorted by magnetic fields applied perpendicular to the tetragonal axis,<sup>3,5</sup> we first attempted to fit just the parallel Zeeman results to a crystal-field calculation.

The crystal-field Hamiltonian for  $f$  electrons in a site of  $D_{2d}$  symmetry, in the Stevens operator equivalent form (applicable only to a single  $J$  manifold), is

$$\mathcal{H} = \alpha(A_2^0 O_2^0) + \beta(A_4^0 O_4^0 + A_4^4 O_4^4) + \gamma(A_6^0 O_6^0 + A_6^4 O_6^4) ,$$

where the reduced matrix elements  $\alpha$ ,  $\beta$ ,  $\gamma$  for the ground  $J$  manifolds of the rare-earth ions and the matrix elements of the operators  $O_n^m$  for various  $J$ 's have been tabulated.<sup>14</sup> The  $A_n^m$  are crystal-field parameters generally obtained by fitting the observed energy levels. This Hamiltonian will split the  ${}^7F_6$  ground manifold of  $\text{Tb}^{3+}$  into three doublets and seven singlets. The origin and character of these ten levels is clear upon examination of the crystal-field matrix, which subdivides as shown in Table I. The matrix elements are given by

TABLE I. Decomposition of the crystal-field matrix of the lowest-lying manifold,  ${}^7F_6$ , of  $\text{Tb}^{3+}$  in  $\text{TbPO}_4$ . The constituent submatrices are given, along with the schematic composition of the states.

Matrix	Representation $\Gamma$ (quantum number $\mu$ )	No. of levels (degeneracy)	Schematic wave function
$\begin{pmatrix} \langle 6  _s   &  6\rangle_s &  2\rangle_s \\ \langle 2  _s   & H_{6,6} & H_{6,2} \\ & H_{6,2} & H_{2,2} + H_{2,-2} \end{pmatrix}$	$\Gamma_4$ ( $\mu = 2^s$ )	2(1)	$ 6\rangle_s +  2\rangle_s$
$\begin{pmatrix} \langle 6  _a   &  6\rangle_a &  2\rangle_a \\ \langle 2  _a   & H_{6,6} & H_{6,2} \\ & H_{6,2} & H_{2,2} - H_{2,-2} \end{pmatrix}$	$\Gamma_3$ ( $\mu = 2^a$ )	2(1)	$ 6\rangle_a +  2\rangle_a$
$\begin{pmatrix} \langle \pm 5   &   \pm 5 \rangle &   \pm 1 \rangle &   \mp 3 \rangle \\ \langle \pm 1   & H_{5,5} & H_{5,1} & 0 \\ \langle \mp 3   & H_{5,1} & H_{1,1} & H_{1,3} \\ & 0 & H_{1,3} & H_{3,3} \end{pmatrix}$	$\Gamma_5$ ( $\mu = \pm 1$ )	3(2)	$  \pm 5 \rangle +   \pm 1 \rangle +   \mp 3 \rangle$
$\begin{pmatrix} \langle 4  _s   &  4\rangle_s &  0\rangle \\ \langle 0   & H_{4,4} & \sqrt{2}H_{4,0} \\ & \sqrt{2}H_{4,0} & H_{0,0} \end{pmatrix}$	$\Gamma_1$ ( $\mu = 0^s$ )	2(1)	$ 4\rangle_s +  0\rangle$
$\langle 4  _a   \begin{pmatrix}  4\rangle_a \\ H_{4,4} \end{pmatrix}$	$\Gamma_2$ ( $\mu = 0^a$ )	1(1)	$ 4\rangle_a$

$$H_{m,m} = \alpha A_2^0 \langle m | O_2^0 | m \rangle + \beta A_4^0 \langle m | O_4^0 | m \rangle + \gamma A_6^0 \langle m | O_6^0 | m \rangle,$$

$$H_{m,m-4} = \beta A_4^4 \langle m | O_4^4 | m-4 \rangle + \gamma A_6^4 \langle m | O_6^4 | m-4 \rangle.$$

The  $s$  and  $a$  indicate symmetric and antisymmetric combinations, respectively, of  $\pm m$ ; e. g.,

$$|6\rangle_s = (|6\rangle + |-6\rangle)/\sqrt{2} \quad \text{and} \quad |6\rangle_a = (|6\rangle - |-6\rangle)/\sqrt{2}.$$

The wave functions, for example, of crystal quantum number  $\mu = 2^s$  will be of the form  $\psi_1 = a|6\rangle_s + b|2\rangle_s$ ,  $\psi_2 = b|6\rangle_s - a|2\rangle_s$ ,  $a^2 + b^2 = 1$ . As a matter of notation, we will refer to wave functions by their largest component. Thus  $|6\rangle_s$  is a  $\mu = 2^s$  state which contains more  $|6\rangle_s$  than  $|2\rangle_s$ .

To obtain a first approximation of where the crystal-field levels of the  $\text{Tb}^{3+} {}^7F_6$  manifold lie, we used the parameters<sup>15</sup> found for  $\text{Er}^{3+}:\text{YPO}_4$ , scaled by the relative radial integrals.<sup>16</sup> The energies calculated from these parameters fall into three groups: four levels from 0 to 40  $\text{cm}^{-1}$ , with major components  $| \pm 5 \rangle$ ,  $|4\rangle_s$ ,  $|6\rangle_s$ , and  $|6\rangle_a$ ; three levels around 90  $\text{cm}^{-1}$  with major components  $|2\rangle_s$ ,  $| \pm 3 \rangle$ , and  $|4\rangle_a$ ; and three levels around 250  $\text{cm}^{-1}$  whose major components are  $|0\rangle$ ,  $| \pm 1 \rangle$ , and  $|2\rangle_a$ , as shown in Fig. 5. We note that the gross order follows  $J_a^2$ , reflecting the large value of  $A_2^0$ .

Our far-infrared data fall into this general scheme, showing several levels below 25  $\text{cm}^{-1}$  and at least two levels around 80  $\text{cm}^{-1}$ . Optical data<sup>17</sup> have confirmed the presence of several levels in the region of 300  $\text{cm}^{-1}$ . From our Zeeman data we conclude that the lowest levels are a  $| \pm 5 \rangle$  doublet and a  $|6\rangle_s$  singlet nearly degenerate with each other, a  $|6\rangle_a$  singlet at about 10  $\text{cm}^{-1}$ , a  $|4\rangle_s$  singlet at 21  $\text{cm}^{-1}$ , a  $| \pm 3 \rangle$  doublet at 75–80  $\text{cm}^{-1}$ , and a

$|2\rangle_s$  and/or a  $|4\rangle_a$  singlet also near 80  $\text{cm}^{-1}$ . This scheme maintains the level groupings found from the  $\text{Er}^{3+}:\text{YPO}_4$  parameters, but reorders the states

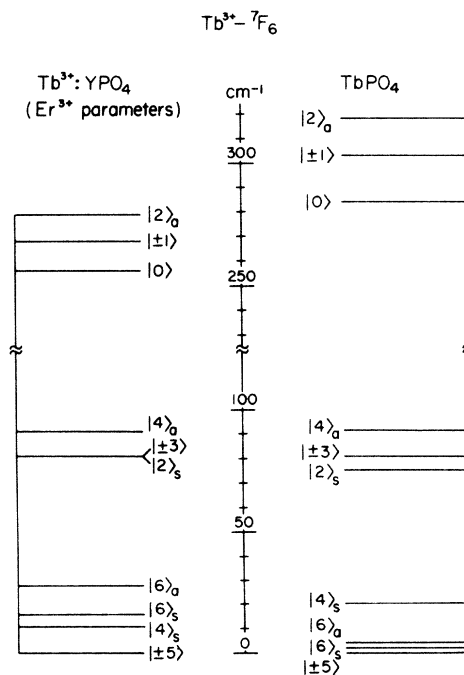


FIG. 5. Calculated energy levels of the lowest crystal-field manifold of  $\text{Tb}^{3+}$ ,  ${}^7F_6$ . The left side was calculated from the parameters determined for  $\text{Er}^{3+}:\text{YPO}_4$  (Ref. 15), scaled by the relative radial integrals (Ref. 16). The right side was calculated from the parameters in Table II, which represent the best fit to our Zeeman data.

within the groups, as shown in Fig. 5. We arrive at this scheme in the following way.

We shall first consider the parallel Zeeman effect. The fastest moving transition shows a high-field splitting factor of  $s = 15.5$ , where  $\Delta E$  (transition) =  $s\mu_B H$ . This is larger than the maximum that could be obtained from a  $|\pm 5\rangle$  state, which is  $s = 15$ , and attempts to force such an identification made it impossible to obtain a satisfactory crystal-field fit for the remaining transitions. It must therefore be a transition between two coupled  $|\pm 6\rangle$  states or between a  $|6\rangle$  and a  $|5\rangle$  state. A fast moving  $|6\rangle$  state can only arise from the  $|6\rangle_a$  and  $|6\rangle_s$  states being close enough together for a large parallel magnetic field to couple them and purify them into  $|+6\rangle$  and  $|-6\rangle$ . We conclude that we have low-lying  $|6\rangle_s$  and  $|6\rangle_a$  states. We must then also have a  $|\pm 5\rangle$  doublet nearby, in order to give the observed perpendicular splitting.

This picture of the  $|\pm 5\rangle$  degenerate doublet and the  $|6\rangle_s$ ,  $|6\rangle_a$  close together is confirmed by examining the transitions that terminate at the 20-cm<sup>-1</sup> line, which we assign as the remaining low state,  $|4\rangle_s$ . There are two such transitions, which cross at 30–40 cm<sup>-1</sup>. The separation of these two transitions thus reflects the separation between the  $|-5\rangle$  state and the  $|6\rangle_s$  purifying to the  $|-6\rangle$  state as the field is increased. We also note that both transitions show curvature toward lower energies at high fields, indicating that the  $|4\rangle_a$  is close enough to the  $|4\rangle_s$  to push it down as their coupling increases in high fields. This confirms that the  $|4\rangle_a$  is one of the middle-region levels. The levels at  $\approx 78$  cm<sup>-1</sup> could be any combination of  $|2\rangle_s$ ,  $|\pm 3\rangle$ , and  $|4\rangle_a$ .

We attempted to find the five crystal-field parameters  $A_n^m$  by fitting the calculated levels to our scheme, including both the zero-field and parallel Zeeman data. We found, however, that a large range of parameters would reproduce the data fairly well, mainly due to the many possibilities for the two transitions originating at  $\sim 78$  cm<sup>-1</sup>. We therefore decided to use the perpendicular Zeeman data as a guide, since there is evidence that the distortion at 4.2 °K in applied perpendicular mag-

TABLE II. Crystal-field Hamiltonian for Tb<sup>3+</sup> in a site of  $D_{2d}$  symmetry. The values given for the crystal-field parameters were determined as described in the text, and used in calculating the energy levels of Fig. 5.

	$A_2^0$	$A_4^0$	$A_6^0$	$A_4^4$	$A_6^4$
$\text{LaF}_3$ : YPO <sub>4</sub>	141.4	18.1	-40.4	$\pm 837.3$	$\pm 88.5$
TbPO <sub>4</sub>	213	25	-43	-1045	-450

TABLE III. Energy and composition of the Tb<sup>3+</sup> $^7F_6$  crystal-field states for the TbPO<sub>4</sub> parameters given in Table II.

$E$ (cm <sup>-1</sup> )	Composition
318	$1.0 2\rangle_a - 0.05 6\rangle_a$
303	$0.79 \pm 1\rangle - 0.61 \mp 3\rangle - 0.13 \pm 5\rangle$
284	$0.85 0\rangle - 0.52 4\rangle_s$
92	$1.0 4\rangle_s$
81	$0.76 \mp 3\rangle + 0.51 \pm 1\rangle - 0.38 \pm 5\rangle$
75	$0.98 2\rangle_s - 0.21 6\rangle_s$
20	$0.85 4\rangle_s + 0.52 0\rangle$
4	$1.0 6\rangle_a + 0.05 2\rangle_a$
2	$0.98 6\rangle_s + 0.21 2\rangle_s$
0	$0.91 \pm 5\rangle + 0.33 \pm 1\rangle + 0.23 \mp 3\rangle$

netic fields  $< 30$  kOe is small when  $H$  is along one of the unit cell axes,<sup>3,8</sup> as it is in our case.

All of the fits to the parallel data give about the same results for the low-lying perpendicular levels, but very different results for the upper levels. From the three transitions originating at 75–80 cm<sup>-1</sup> we conclude that the  $|\pm 3\rangle$  level and either the  $|2\rangle_s$  or  $|4\rangle_a$  (but not both) are located there. Crystal-field calculations indicated that it is the  $|2\rangle_s$  level in this location with the  $|4\rangle_a$  higher. Our calculated energy levels for parallel and perpendicular fields are shown in Figs. 3(a) and 4(a), along with the data and the calculated transition [Figs. 3(b) and 4(b)] for the crystal-field parameters given in Table II. The zero-field energies and wave functions for these parameters are given in Table III.

Figures 3(b) and 4(b) show that the fit is very good for the parallel Zeeman data and reasonable for the perpendicular data. Furthermore, the highest levels at  $\approx 300$  cm<sup>-1</sup> are in good agreement with the optical data. The fit to the perpendicular Zeeman data in high fields could be improved by moving the  $|4\rangle_a$  level higher, decreasing its coupling to the  $|3\rangle_a$ . Attempts to achieve this, however, necessitated lowering the upper levels to  $\approx 250$  cm<sup>-1</sup>. It should be remembered, moreover, that the effects of the magnetically induced crystalline distortion in high perpendicular fields are not known, and could materially affect the calculated results.

One additional comment must be made on the crystal-field fit. It can be seen by examining the matrices in Table I that if the signs of the off-diagonal parameters  $A_4^4$  and  $A_6^4$  are reversed, the crystal-field energies remain the same. The  $\mu = 2^s$  and  $\mu = 2^a$  states, however, are interchanged (also signs within the wave functions change). The changes make no difference to the parallel Zeeman

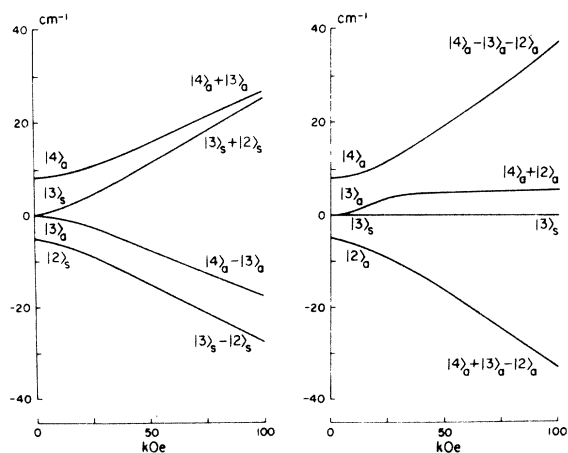


FIG. 6. Schematic illustration of the perpendicular Zeeman behavior of the crystal-field levels located at  $\approx 80 \text{ cm}^{-1}$  for the two different choices of symmetry assigned to the  $|2\rangle$  state, as dictated by the signs of the off-diagonal crystal-field components.

interaction, which couples only those states within the same crystal quantum number. Thus a parallel Zeeman fit can determine only the relative signs of  $A_4^4$  and  $A_6^4$ . There is a difference, however, in a perpendicular field, which mixes symmetric states among themselves and antisymmetric states among themselves. Thus for one sign convention, for example, the middle states would be  $|2\rangle_s$ ,  $|\pm 3\rangle$ , and  $|4\rangle_a$ , and for the other  $|2\rangle_a$ ,  $|\pm 3\rangle$ , and  $|4\rangle_a$ . The difference in their behavior in a perpendicular field is illustrated schematically in Fig. 6. There are similar but less dramatic effects in the low-energy group, where the coupling is  $|6\rangle_s$ ,  $|5\rangle_s$ ,  $|4\rangle_s$  and  $|6\rangle_a$ ,  $|5\rangle_a$ . In the two cases the energies of the  $|6\rangle_s$  and  $|6\rangle_a$  are reversed. In the second case we would require all three levels close together to obtain perpendicular splittings such as we observed. However, the first sign convention with the  $|4\rangle_a$  state moved higher reproduces the qualities of the perpendicular spectra more satisfactorily.

We have ignored the effects of internal magnetic fields (dipole and exchange) in fitting our high-field data. The dipolar fields in the parallel saturated state can be estimated from those in  $\text{DyPO}_4$ ,<sup>18,19</sup> scaled down by the ratio of the moments. This indicates that the saturation dipolar fields in slabs of  $\text{TbPO}_4$  are on the order of 2 kOe. The shift of the levels in the optical spectrum when cooled below the ordering temperature is about  $3 \text{ cm}^{-1}$ .<sup>3,6,9</sup> This indicates (for  $g \approx 16$ ) a saturation exchange field of about -4 kOe, giving a total for the internal fields at saturation of -2 kOe. This is less than the accuracy of our crystal-field fit, and thus has been neglected.

## V. DISCUSSION

The important feature of our energy-level scheme is that there are not just one, but two low-lying magnetic doublets, one degenerate ( $|\pm 5\rangle$ ), and one nondegenerated ( $|6\rangle_s$  and  $|6\rangle_a$ ). This means that the magnetic properties are determined by the competition between these two doublets. We see, in fact, that in a parallel field the  $|-5\rangle$  and  $|-6\rangle$  states cross over and remain close together up to quite high fields. This feature is probably the cause of most of the inconsistencies in the previous work reported by others. The large linewidths and asymmetries in the optical spectra could arise from overlapping transitions originating from both of these low levels, whose relative population will depend upon both temperature and applied field. The parallel  $g$  factors which are measured will differ, depending upon which level is the ground state of the transition. For the  $|6\rangle$  doublet,  $g_{\parallel}$  also depends on how high the fields are, since the  $|6\rangle_s$  starts with a  $g$  factor of 0, which increases to about 16 in high fields as the state becomes  $|-6\rangle$ . Also in perpendicular fields the slopes of the levels change with field as levels are mixed together. The reported magnetization measurements were done only in low fields, where even at low temperatures saturation has not been reached.

Sivardière<sup>20</sup> did a molecular-field analysis of the Jahn-Teller distortion and antiferromagnetic ordering in  $\text{TbPO}_4$ , using the model of a low doublet and singlet only. He concluded that for this model the magnetic ordering could occur at a canted angle (as observed in neutron-diffraction studies) only if the distortion were monoclinic. He suggests, however, that the distortion could be orthorhombic if there was another low singlet. We now have evidence that indeed there is a second low singlet, which thus allows the possibility of the distortion being orthorhombic.

Although we now have a much better understanding of the behavior of  $\text{TbPO}_4$ , some details must still be pinned down. We do not know precisely what the separation of the low doublet and two singlets are since these small energy differences are outside of the spectral range of our apparatus. Measurements of both these levels and the high-energy levels in the  $300\text{-cm}^{-1}$  range would enable a more accurate crystal-field fit, and perhaps warrant including the effects of the next manifold,  ${}^7F_5$ . High-field magnetization measurements at various temperatures would give a better picture of the spacings and moments of the two competing levels, and also a saturation value for the high-field moment of the  $|6\rangle$  state. The general picture of the low-lying energy-level structure is now clear, however, and a starting point has been established for understanding the crystalline distortion and the magnetic ordering.

- \*National Research Council-Naval Research Laboratory, Research Associate.
- <sup>1</sup>J. L. Lewis and G. A. Prinz, AIP Conf. Proc. 18, 298 (1974).
- <sup>2</sup>R. W. G. Wyckoff, *Crystal Structures*, 2nd ed. (Interscience, New York, 1965).
- <sup>3</sup>J. N. Lee and H. W. Moos, Solid State Commun. 9, 1139 (1971).
- <sup>4</sup>H. C. Schopper, P. J. Becker, W. Böhm, G. Dummer, H. G. Kahle, L. Klein and G. Müller-Vogt, Phys. Status Solidi B 46, K115 (1971).
- <sup>5</sup>H. C. Schopper, Int. J. Magn. 3, 23 (1972).
- <sup>6</sup>S. Spooner, J. N. Lee, and H. W. Moos, Solid State Commun. 9, 1143 (1971).
- <sup>7</sup>J. Coing-Boyat (unpublished), referenced in H. C. Schopper, Int. J. Magn. 3, 360 (1972).
- <sup>8</sup>J. N. Lee and H. W. Moos, Phys. Rev. B 5, 3645 (1972).
- <sup>9</sup>W. Böhm, R. Herb, H. G. Kahle, A. Kasten, J. Laugsch, and W. Wüchner, Phys. Status Solidi B 54, 527 (1972).
- <sup>10</sup>G. T. Rado and J. M. Ferrari, AIP Conf. Proc. 10, 1417 (1973).
- <sup>11</sup>Fourier spectrophotometer, model No. 720, manufactured by Research and Industrial Instruments Corp., London, England.
- <sup>12</sup>T. Y. Chang, T. J. Bridges, and E. G. Burkhardt, Appl. Phys. Lett. 17, 249 (1970).
- <sup>13</sup>R. J. Wagner, A. J. Zelano, and L. H. Ngai, Opt. Commun. 8, 46 (1973).
- <sup>14</sup>M. T. Hutchings, Solid State Phys. 16, 227 (1964).
- <sup>15</sup>D. Kuse, Z. Phys. 203, 49 (1967).
- <sup>16</sup>A. J. Freeman and R. E. Watson, Phys. Rev. 127, 1058 (1962).
- <sup>17</sup>J. N. Lee, dissertation (The Johns Hopkins University, 1971) (unpublished).
- <sup>18</sup>G. A. Prinz, J. F. L. Lewis, and R. J. Wagner, Phys. Rev. B 10, 2907 (1974).
- <sup>19</sup>J. C. Wright, H. W. Moos, J. H. Colwell, B. W. Mangum, and D. D. Thornton, Phys. Rev. B 3, 843 (1971).
- <sup>20</sup>J. Sivardière, Phys. Rev. B 8, 2004 (1973).